Operando SXRD : a new view on catalysis

Ackermann, M.D.

I: Introduction and Theory

1.1: Introduction

Surface Science is a part of Solid State physics. Although surfaces seem to only represent a small part of a solid crystal, many physical and chemical processes take place at surfaces. Surfaces can very generally be defined as the plane where two different materials or two different phases of one material are in contact with each other. The contact between two phases of the same material might induce stress, which will influence the shape of the surface; the contact between different materials at a surface might result in a chemical reaction at the surface involving two or more of these materials[i].

In this thesis I will concentrate on metallic surfaces in contact with a gas phase, and especially on the processes that occur on the atomic level at the metal surface when brought into contact with one or more gaseous species. In the work present in this thesis, we have focused on two main processes that occur when a metal surface is brought into contact with molecules or atoms in the gas phase: The surface itself might be structurally or chemically altered, and the molecules in the gas phase can be altered. The first process can be the roughening or oxidation of a metallic surface, and falls in the domain of surface science. The second process, in which a surface plays a role in the chemical altering of the gas phase, would by many be considered catalysis. Throughout our research, we have tried to link the one with the other: How can we link morphological or chemical changes in the surface of a metal (i.e. the catalyst) to changes in the chemical composition in the gas phase (i.e. the catalytic process). By understanding the link between the changes in or on the surface and the changes in the catalytic reaction, we try to unravel the atomic pathway of the molecules that adsorb onto, react and desorb from the catalysts surface. The main technique we have used to unravel this process is *Surface X-Ray Diffraction* (*SXRD*). This technique has been used for many years already to gather atomically detailed information about the surface structure and composition of solids. The novelty is that we can perform *SXRD* experiments

---

[i] *This specific discipline of chemical reactions between a gas and a solid, which falls within the field of surface science, is commonly called surface chemistry. One of the pioneers of surface chemistry, Gerhard Ertl, was awarded the Nobel Prize in chemistry in 2007 for his contribution to the understanding of the interaction between gasses and solid surfaces.*

while the catalytic reaction is actually running, i.e. while the catalyst is operating, making this *Operando SXRD*.

In this first chapter I will give an introduction into the basic processes of heterogeneous catalysis, the influence of gasses on surfaces and the techniques we and others have used to investigate the surface of catalysts. To understand the data, results and conclusions presented later on in this thesis, I will also give an introduction to the atomic structure of surfaces. I will introduce the formalism used to describe surfaces on the atomic level, and use this to explain the basic principles of *Surface X-Ray Diffraction*.

1.2: Heterogeneous catalysis

1.2.1: Catalysts

A catalyst is a substance that accelerates a chemical reaction, without itself being consumed by this same reaction. In heterogeneous catalysis, the catalyst is in another state than the reactants, e.g. a solid catalyst in contact with a reactant gas mixture. The oldest (1909) large scale application of heterogeneous catalysis is the formation of ammonia, a substance extensively used in fertilizers and indispensable for modern agriculture by Fritz Haber and Carl Bosch [1].

With a solid catalyst the reaction generally takes place at, or within several atomic distances of the catalysts surface. The catalyst surface can play several roles in order to accelerate the reaction.

1) The surface offers a 2D matrix of adsorption sites which acts as a simple trap where the chance for the different species from the gas phase to come into contact with each other is much greater than in the gas phase.
2) The catalyst surface alters (lowers) the energetic barrier that must be overcome to go from the reactants to the reaction product. This effectively lowers the temperature at which the reaction will run, or equivalently accelerates the reaction at a given temperature, as long as the original energetic barrier was larger or in the order of kT.
3) The catalyst surface alters one or more of the reactants, creating an intermediate species which is necessary for the reaction to run. This is for example the case with dissociative adsorption: where atomic oxygen is virtually absent in the gas phase at 500K in 1 bar of O_2, it is present due to dissociative adsorption on the surface of catalysts employed for CO oxidation in these conditions.

In all cases one or more species from the gas phase adsorb onto the catalyst surface, diffuse on the surface, react, and leave the surface in the form of the reaction product. All three processes just mentioned depend strongly on the interaction between the molecules from the gas phase and the surface, which as mentioned earlier is determined by the specific adsorption energy of a certain

molecule or atom with a specific surface. In the combination of adsorption and subsequent desorption of the molecules lies a balance between high and low adsorption energy. For very high adsorption energies, the surface will accumulate many reactants, but might be very slow in releasing the reaction product, effectively blocking the surface for the adsorption of new reactants. For very low adsorption energies, the reactants might adsorb and desorb so rapidly that they will leave the surface before reacting to the reaction product. This effect is often plotted in so called 'volcano plots' where the reactivity is plotted versus the binding energy of different catalyst. The optimal catalyst, at the top of the volcano curve, is the one with the correct balance between adsorption and desorption for the reactants and reaction product [2,3].

1.2.2: Reaction mechanisms

One of the simplest catalytic reactions is one in which two molecules form the gas phase, the reactants labeled *"A"* and *"B"*, come in contact with the catalyst and react under formation of the reaction product *"AB"*.

$$A + B \xrightarrow{Catalyst} AB \qquad (1)$$

I will present three different reaction pathways or mechanisms in which such a simplified catalytic reaction can occur. The most common reaction mechanism is called the Langmuir-Hinshelwood (LH) mechanism. In this mechanism both particles *A* and *B* adsorb on the surface of the catalyst, which is assumed to be a perfectly flat isotropic surface, consisting of fully equivalent adsorption sites for both *A* and *B*. *A* will react with *B* under formation of *AB* with a probability *k*, whenever an adsorbed *A* finds an adsorbed *B* as its neighbor on this surface. The chance of this happening, will depend on the coverage θ of both *A* and *B* (labeled respectively θ_A and θ_B). Assuming that this is the rate limiting step, the reaction rate *R* will be a function of *k*, θ_A and θ_B:

$$R(\theta_A, \theta_B) = k \cdot \theta_A \cdot \theta_B \qquad (2a)$$

where the total number of adsorption sites has been normalized to 1, and θ_A and θ_B hence run from 0 to 1. For elevated pressure conditions we can assume the surface to be almost fully covered by adsorbed species, and hence that $\theta_A + \theta_B = 1$. The maximum in reactivity is then reached at $\theta_A = \theta_B = 0.5$, and the reaction rate shows a quadratic decay for changes in both θ_A and θ_B.

As it is more difficult to measure and regulate coverages than gas pressures, it is interesting to translate this to the dependence of R on the partial pressures of A and B P_A and P_B, instead of θ_A and θ_B. For this we have to insert in equation (2a) the probability for a particle of type A or B to go from the gas phase to the adsorbed state. We can do that by taking into account the ratio K_i between the sticking coefficient of each species, respectively k_1 and k_2 and desorption coefficients k_{-1} and k_{-2}, where $K_i = k_i / k_{-i}$ and the available amount of free adsorption sites. This results in equation 2b [2,3]:

$$R(P_A, P_B) = k \cdot \frac{K_1 P_A \cdot K_2 P_B}{(K_1 P_A + K_2 P_B + 1)^2} \qquad (2b)$$

The maximum in reaction rate is hence not at $P_A = P_B$ but depends on K_1 and K_2 (see figure 1) This equation can easily be rewritten for a different stoichiometry, or for e.g. dissociative adsorption for molecules like O_2 (see e.g. chapter 5).

Another common reaction pathway is the Eley-Rideal (ER) mechanism. In this mechanism, only one of both species is adsorbed on the surface. The reaction takes place when the adsorbed species A comes into contact with a particle B from the gas phase. In this case the reaction rate depends on the coverage θ_A and the impingement rate of B, which is directly proportional to the partial pressure P_B:

$$R(\theta_A, P_B) = k \cdot \theta_A \cdot P_B \qquad (3a)$$

In this case R is always linear with P_B, and there is no competition between A and B for adsorption sites. The maximum reaction rate is achieved for $\theta_A = 1$ and is then only dependent on P_B. Translating this to partial pressures this gives:

$$R(P_A, P_B) = k \cdot P_B \cdot \frac{K_1 P_A}{K_1 P_A + 1} \qquad (3b)$$

A last class of reactions which is similar to the ER mechanism is the so-called Mars - Van Krevelen (MvK) mechanism [4]. In this mechanism one of the species A forms a compound with the catalyst "CA", which then acts as a source for the other species (B) to react with. An example of this would be the formation of an oxide with oxygen from the gas phase, or a carbide from CO of CH_4 with a metallic catalyst [5-7,9,10,13,23,36]. Of course, for this to remain a

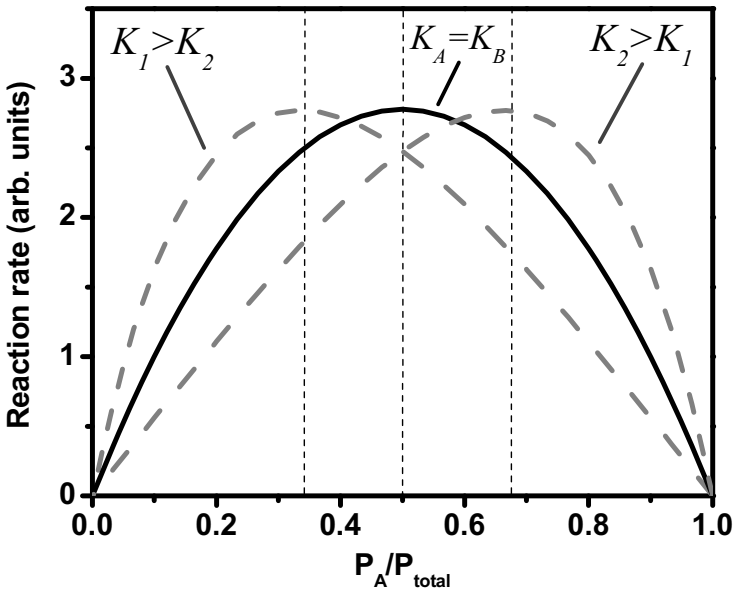

Figure 1: *Reactivity as a function of partial gas pressure P_A, with respect to the total pressure $P_{total} = P_A + P_B$. The reaction rate is maximized at $P_A = P_B$ for equal sticking coefficient and desorption rate K_A and K_B. For $K_A > K_B$ the maximum will shift to left and equivalently to the right for $K_B > K_A$. The catalyst is A-poisoned for $P_A/P_{total} = 1$, and B-poisoned for $P_A/P_{total} = 0$, showing 0 reaction rate in both cases.*

proper catalytic reaction the catalyst part of the compound is released back in its original form after the reaction product has been formed.

$$A + C \longrightarrow AC$$
$$B + AC \longrightarrow AB + C \qquad \textit{(4a / 4b)}$$

Again, the reaction rate depends on the different coverages and partial pressures of the reactants, assuming that there is an abundance of catalyst particles to form the compound with. Assuming that equation (4b) contains the rate limiting steps, the reaction rate can be written as:

$$R(\theta_{AC}, P_B) = k \cdot \theta_{AC} \cdot P_B \qquad \textit{(5)}$$

Comparing this equation to (3a) immediately shows that the reaction rate behaves exactly as for the ER mechanism: independent of θ_{AC} as long as it is near 1, and linear with P_B in all circumstances.

1.3: The Pressure Gap:

1.3.1: Surface Science at elevated pressure and temperature

The pressure gap is the name given for the large difference in pressure between the traditional surface science experiments performed in UHV, and the typical pressures at which most catalysts actually operate. Where traditional UHV experiments are performed at pressures of typically 10^{-9} to 10^{-6} mbar, the operation conditions for most catalysts are in the order 1 and 100 bar. The pressure gap hence represents a difference of 10 to 12 orders of magnitude in pressure.

1.3.2: Chemical potential: influence on surface structure

We define a system where a (metal) sample, consisting of a surface and a bulk is in contact with a gaseous environment. According to thermodynamics, the system will always try to minimize its free energy *G*. This energy depends on the free energy of the bulk G_{bulk}, the free energy of the surface G_{surf}, and the free energy of the gas G_{gas}[ii]:

$$G = G_{surf} + G_{gas} + G_{bulk} \qquad (6)$$

Assuming that the bulk structure (and hence free energy) will not change due to the interaction of the sample with the gas phase, the system has no freedom to minimize its energy by changing G_{bulk}. We will hence focus on G_{surf} and G_{gas}. G_{gas} is a directly linked to the chemical potential of the individual species in the gas phase. For each type of molecule '*i*' in the gas phase we can define $G_{i\ gas}$ as $N_i \cdot \mu_i$, with N_i the number of molecules of type *i* in the gas phase, and μ_i the chemical potential of that particular molecule. μ_i is defined as the amount of energy by which the total system would change if an additional particle of type *i* were introduced into or removed from the gas phase (with the entropy and volume held constant). If a system contains more than one type of molecules,

[ii] *The full description of the energy of a system should also incorporate an extra term related to entropy, but it has been omitted here for simplicity.*

G_{gas} is equal to the sum of the separate chemical potentials associated with each species multiplied by the number of molecules of that species, i.e. $N_i \cdot \mu_i + N_j \cdot \mu_j + \ldots$. We can calculate μ_i for a given particle of type i with a partial pressure P_i at a given temperature T:

$$\mu_i\left(P_i\right) = kT \cdot \ln\left(P_i / P_i^0\right) \tag{7}$$

where k is the Boltzmann constant and P_i^0 is a tabulated value for particles of type i which depends mainly on the mass of that particular molecule and the temperature T. We note that μ_i is always negative, otherwise the gas would spontaneously condensate. This means that for all temperatures P_i must be smaller than P_i^0. We also note that μ_i is exactly the amount of energy it costs to remove one single particle from the gas phase. According to equation (7) this value decreases with increasing pressure. It becomes energetically increasingly favorable (less costly) to take molecules from the gas phase as P_i increases.

We now compare two states in which the system can be. In the first state the surface is purely metallic ($G_{surf} = G_{metal}$) and N molecules of type i are in the gas phase. In the other case the surface forms a new structure with the molecules from the gas phase ($G_{surf} = G_{metal+i}$), incorporating n molecules form the gas phase. Assuming that $N >> n$, we can write down the free energy for both cases:

$$1:\ G_1 = G_{metal} + N_i\mu_i\left(P_i\right) + G_{bulk} \tag{8a}$$

$$2:\ G_2 = G_{metal+i} + \left(N_i - n\right)\mu_i\left(P_i\right) + G_{bulk} \tag{8b}$$

To predict which state has the lowest (total) free energy, we have to calculate which free energy will be lower. The difference between both states is:

$$\Delta G = G_{metal} - \left(G_{metal+i} - n\mu_i\left(P_i\right)\right) \tag{8c}$$

or in other terms: The system will go from the *metal* to the *metal+i* state when ΔG is exactly 0:

$$G_{metal} = G_{metal+i} - n\mu_i\left(P_i\right) \qquad (8d)$$

Keeping in mind that $\mu_i(P_i)$ is negative, we see that the surface that incorporates the molecules from the gas phase will only form when P_i is high enough that the cost of removing the molecules from the gas phase is smaller than the gain in energy for forming the new surface structure. Equation 7 shows that this becomes increasingly easy at higher partial pressures (for a fixed temperature). The factor 'n' scales with the stoichiometry of the structure formed: if for a layer of PdO we take n to be 1, n will be 2 for PdO_2 as for forming 1 layer of PdO_2 twice as many molecules need to be taken from the gas phase. In essence, equations (7) and (8d) show that higher pressures will favor structures which incorporate more molecules from the gas phase; structures which are not stable, i.e. do not represent the lowest free energy at lower pressures. The difference in free energy between UHV conditions (e.g. $P_i = 10^{-7}$ mbar) and elevated pressure conditions ($P_i = 1000$ mbar) bar for a structure that incorporates 1 molecule form the gas per unit of surface area will be $kT \cdot \ln(10^{10}) \cong 23\ kT$. At room temperature this is equal to 0.58 eV per unit of surface area, or per adsorbed molecule. This energy gain scales linearly with the stoichiometry or '*n*' [28,29].

1.3.3: Kinetic barriers: Low versus high temperature and pressure

According to equation (7), decreasing *T* will have the exact same effect on μ_i and hence on the stability of a phase as increasing the pressure. This suggests that experiments performed in UHV will show the same structures as experiments performed at ambient pressures, as long as UHV pressures are combined with low (cryogenic) temperatures[iii]. As many techniques used in Surface Science do not work at elevated pressures, research has often used this 'trick' to be able to study adsorption structures in UHV. This combination of low temperature and UHV does indeed allow surface scientists to form and

[iii] *A quick look at the example given above shows that to match the chemical potential of an experiment performed a 1000 mbar and room temperature (300 K) one would need to go to 13 K for a pressure of 10^{-7} mbar.*

study adsorption structures with UHV-based techniques, but it has several drawbacks. Firstly, the formation of a certain structure will always involve overcoming a certain kinetic barrier, independently of the total free energy. When working at low temperatures, the energetically most favorable structure might not form because the kinetic barrier is much larger than kT. Instead, the system will exhibit a surface structure with a low kinetic barrier, but which is *not* the thermodynamic equilibrium.

Secondly, the surface cannot react to changes in the chemical potential, as due to the low temperature it is 'stuck' in this local energy minimum. The effect of this is that the *order* in which the surface is exposed to different gas species is fully determining for the state of the surface, and not the actual gas composition [13].

Especially in the case of gas *reactions* on surfaces, i.e. heterogeneous catalysis, the surface structure can be very dynamic. Gas molecules impinge on the surface, are adsorbed and altered, and subsequently leave the surface under formation of reaction products. For a catalytic reaction to run, the energetically most favorable condition must be the one with the reaction product forming on and desorbing from the surface. As long as the reaction is running, the structure of the surface is hence always partly determined by kinetics, as well as thermodynamics. A catalytically active system is hence intrinsically a system of which the structure is strongly dependent on the rate of the different processes, and hence very sensitive to the temperature.

There are hence two main reasons why surface structures found in low temperature UHV-studies can generally not be extrapolated to high pressure and temperature conditions with the same μ_{gas}.

4) Kinetic barriers can prevent the structure which represents the actual thermodynamic equilibrium to form on the timescale of an experiment at low temperatures.

5) The kinetic processes involved in the catalytic reaction can influence the structure on the surface. An effect that will not be seen if the catalytic reaction does not run.

The only way to determine the surface structure of a catalyst during its active phase is therefore to actually measure the structure *in-situ*, while the reaction is running, i.e. under high temperature and pressure conditions.

1.4: The Materials Gap

Next to the pressure gap, the surface chemistry community also struggles with a problem named the 'materials gap'. The materials gap is the name commonly given to the difference between model catalysts consisting of large, flat, clean single crystal surfaces and real (industrial) catalysts, consisting of (alloy) nano-particles on oxide supports, using different types of promoters. The most important reason to make a (real-life) catalyst out of small metallic particles deposited on an oxide support is to maximize the total surface of the catalytically active material (the metal), while minimizing its volume. This is to improve the total reaction rate (high surface area) and the cost efficiency (low mass), as the catalytically active metals are commonly much more expensive than the oxides used as support material. Promoters are added to improve the catalysts reaction rate, selectivity, or even lifetime. Unfortunately, such complicated systems consisting of small particle, oxide supports, promoters and more are often too complicated to study in surface science experiments. Experiments of most surface science techniques require that the samples used are single crystal surfaces, looking at the interaction of the top layer of a single bulk metal sample and the gas phase only. This is commonly called a 'model catalyst' and is crude simplification of a real life catalyst.

Two main effects that can have an influence on the chemical properties of the particles, are the size and shape of the particle itself, and the interaction of the particle with the oxide support or promoters. If the particle size becomes of the order of the wavelength of the electrons found inside the particle, the electronic properties of the particle start to change. The alteration of the electronic properties can have a strong effect on the reactivity of the particles, like has been observed on Au nano-particles [14]. The second effect is that a nano-particle has relatively much more atoms at edge, kink and step-positions than a single crystal surface. If these 'special' sites play an important role in the catalytic pathway, the reactivity of a single crystal surface might be almost 0. And finally: the surface of a nano-particle will often consist of differently orientated low index facets. If presence of the different facets in each others vicinity, or the communication between the facets is important for the reaction, small particles will behave very differently from single crystal surfaces.

The other influence might come from the interaction between the oxide support or promoters and the metallic particles. For one, both support and promoters

can alter the electronic structure and hence catalytic properties of the particles. Secondly, similarly to the edge and kink sites, the boundary between the oxide support and metal particle might be a 'special' site with respect to the reaction pathway [15]. The same problems play in extrapolating single crystal results to small particles as in extrapolating results from low temperature / low pressure experiments to realistic conditions. The aim of our future research is to be able to bridge both the pressure gap and the materials gap in one single setup. A future High Pressure *SXRD* setup, which is under development in collaboration between Leiden University and the ID03 beamline of the ESRF is specifically aimed at achieving this goal.

1.5: Techniques for studying surfaces under elevated pressure conditions

1.5.1: The conflict of surface sensitivity and elevated pressures

In order to be sensitive to the surface of a macroscopic crystal, information carriers (photons, electrons or ions) need to have a relatively large interaction cross-section with the atoms at the surface of the crystal. If not, most of them will penetrate into the bulk and hence yield information about the bulk. Recovering information about the surface of the crystal from the measured signal will therefore be relatively difficult. Low energy electrons and ions are hence much better suited to determine surface properties, and are used in most traditional surface science techniques (e.g. LEED, LEIS, LEEM [16]). Unfortunately, the high cross-section with the surface atoms also implies a high cross-section with gas molecules. This results in a very short mean free path for low energy electron and ions in an elevated pressure environment. It is thus intrinsically difficult to develop techniques that are very sensitive for surfaces and will operate well in ambient pressure conditions. Despite this difficulty, several techniques have been developed during the last 10 years that can yield very detailed information about the surface structure under high pressure conditions.

1.5.2: Hard X-Rays

Hard X-Rays (photons with a wavelength typically between 1 and 0.1 Å or equivalently an energy between 10 and 100 keV) have, in contrary to what is stated here above, a very low chance of interacting with surface atoms. Because of this, crystallography techniques utilizing hard X-Rays, like X-Ray Diffraction, are better suited for investigating bulk structures rather than surfaces. Surface X-Ray Diffraction (*SXRD*) is a diffraction technique which uses hard X-Rays, but which by the use of several geometrical and optical 'tricks', can be made very sensitive to changes in the surface structure and composition. This technique is comparable to Low Energy Electron Diffraction (LEED). The low energy electrons used in LEED have a much stronger interaction (higher cross-section) with matter than the hard X-Rays used in *SXRD*. Because of this LEED is intrinsically more sensitive to surfaces than *SXRD*. Therefore LEED will in many cases yield more data on the surface structure in a shorter amount of time, which should result in a better surface structure determination. Despite this, *SXRD* has a number of specific advantages with respect to LEED. The lower cross-section of the X-Rays with matter results in a much deeper penetration depth, and hence yields information on the crystal structure up to larger depths within the crystal. This gives the possibility to study the out-of-plane structure of relatively thick crystal layers, and to study e.g. buried interfaces. Secondly, due to the low interaction with matter, X-Rays are almost unaffected by a gas phase surrounding a sample. This makes *SXRD* very well suited for studying surfaces under high pressure conditions [17,39,43]. A thorough and more formal description of *SXRD* is given later in this chapter (see **1.6**).

Extended X-Ray Adsorption Finestructure Spectroscopy (EXAFS) is a technique which is sensitive to the (chemical) surroundings of an atom [17]. By looking at the changes in the fine structure of adsorption edges of the atoms, one can detect changes in the type and number of neighbors that surround an atom. This technique is equally insensitive to the presence of a gas phase surrounding a sample as XRD. Unfortunately it is, like XRD, intrinsically a bulk sensitive method due to the use of hard X-Rays. By using a low incidence angle the contribution from the bulk can be reduced, and the technique is referred to as Surface EXAFS (or SEXAFS) [18], but no interference effects can be used, like in *SXRD*, making the bulk contribution still relatively large with respect to the surface signal.

1.5.3: (High Pressure) Scanning Tunneling Microscope

Scanning Tunneling Microscopy is a technique that was developed in 1986 by Binnig and Rohrer [19]. It consists in scanning the surface with the atomically sharp end of a conducting needle. By applying a small voltage between the needle and the surface, a small current will flow between the surface and the needle, even before the needle actually touches the surface due to tunneling of the electrons through the small gap between the needle and surface. This tunnel current depends strongly on the distance between the needle and the surface[iv]. By keeping the current constant with a feedback system the needle will stay at a constant height above the surface. By scanning the surface in this "constant height mode", and registering the vertical position at every point, we can reconstruct a two dimensional height map of the surface. A Scanning Tunneling Microscope (STM) can do this with a subatomic resolution both in the vertical as in the lateral direction.

This technique is commonly used in UHV conditions, mainly to keep the surface in an atomically clean state. There is no physical limitation to employ this technique at elevated pressures, and several groups have already done this in the recent past [20,21] by filling a complete vacuum system equipped with a standard STM up to the required pressure. To image the surface of a catalyst with an STM *in-situ* while the catalytic reaction is actually running demands a more dedicated approach. Such a dedicated STM has been developed by P.B. Rasmussen, B.L.M. Hendriksen and J.W.M. Frenken [22,23]. This STM is capable of imaging a surface under semi-realistic reaction conditions of 425 K, up to 5 bar of gas and a flow of up to 10 ml_n/min combined with a reactor volume of 0.5 ml. This STM is built into a vacuum system and the reactor is connected to a dedicated gas manifold. The gas flow, and hence the catalytic activity is constantly monitored by a mass spectrometer. Some data measured with this STM by B.L.M. Hendriksen are shown in chapter 5, in combination with *SXRD* measurements. A more thorough description of this setup can be found in the thesis of B.L.M. Hendriksen [23].

[iv] *The tunnel current also depends on the density of states in both the needle as the surface, but when tunneling from a metallic tip onto a metallic surface, this effect is not very important. When tunneling into oxides or semiconductors this effect is of much greater importance.*

1.5.4: A short path through the gas phase

To overcome the problem of the short mean free path of electrons and ions in elevated pressure conditions some research groups have developed setups in which the traveled path of the electrons and ions through the gas phase is very short. One way to do this is to use differential pumping. One of the techniques to which this has successfully been applied is X-Ray Photoelectron Spectroscopy (*XPS*). Although the incoming X-Rays have little interaction with the gas phase, the outgoing photoelectrons are strongly adsorbed by the gas phase. By using the combination of differential pumping, a very small reactor volume and electrostatic lenses, enough photoelectrons can still be collected in pressures up to approximately 50 mbar [24,25].

Another technique that uses this combination of small reactor volumes and differential pumping to minimize the path length through the gas phase is Transmission Electron Microscopy (TEM) [26]. This is a direct imaging technique which is not particularly sensitive to surfaces. But when using samples that consist of nanoparticles, and the image contains several of these particles, one can always observe a good ratio of the atoms within one TEM image to be at the surface of the particles.

1.5.5: Polarization (filtering)

Several optical techniques use optical properties of the surface to be able to differentiate the signal coming form the gas phase, and the signal coming from the surface of the catalyst. The fact that the interaction with the surface changes the polarization of a polarized IR signal is used in a variety of Polarization Modulated IR techniques [27].

Another optical ‘trick’ is to use two different laser sources, and letting them interact at the surface of a sample. A small part of the outgoing signal will consist of photons with a frequency equal to the sum frequency of both laser sources. That signal is very weak, but surface specific. By using high intensity lasers and very sensitive detectors, this technique of Sum Frequency Generation (SFG) is very suited to investigate the chemical composition of a surface under high pressure conditions.

1.5.6: Density Functional Theory

Density Functional Theory (DFT) is a theoretical technique that aims at calculating the free energy G_{surf} of a certain surface structure. By comparing the calculated G_{surf} of different structures, this technique can make predictions about the (thermodynamic) stability of different surface phases [11,12]. In recent work, the influence of the chemical potential of the surrounding gas phase has been added to DFT calculations, allowing scientist to compare the relative stability of different surface structures over a large pressure and temperature range. By doing this for several different surface structures, this addition to DFT calculations can help predict which structure is expected to be the most favorable in terms of free energy for a surface within a wide *(P,T)*-range in the presence of one or multiple species of molecules in the gas phase [28,29].

1.6: Surfaces of metals on the atomic scale

We start this section with a brief overview of basic surface crystallography, which we will make frequent use of throughout this thesis, and which forms the basis for the introduction to *SXRD*.

1.6.1: Unit cells and the bulk structure of crystals

The most common way to describe a crystal structure is to define the so-called unit cell [30]. The unit cell of a crystal is a small 3D volume spanned by the vectors $\boldsymbol{a_1}$, $\boldsymbol{a_2}$ and $\boldsymbol{a_3}$, called the unit vectors. By reproducing the unit cell in the direction of $\boldsymbol{a_1}$, at the positions $n_1 \cdot \boldsymbol{a_1}$ with $n_1 = (-N_1, \ldots -1, 0, 1 \ldots, N_1)$ we get a 1D crystal of length $2 \cdot N_1$. Similarly reproducing the unit cell at $n_2 \cdot \boldsymbol{a_2}$ and $n_3 \cdot \boldsymbol{a_3}$ and linear combinations of these, results in a 3D crystal of dimensions $8 \cdot (N_1 \cdot N_2 \cdot N_3)$, with unit cells at $(n_1 \cdot \boldsymbol{a_1}, n_2 \cdot \boldsymbol{a_2}, n_3 \cdot \boldsymbol{a_3})$. Any volume which by periodic repetition correctly reproduces the full crystal structure is a correct unit cell. The 'primitive' unit cell is the smallest possible unit cell, that still contains all elements to describe the whole crystal structure. In some cases, it is more convenient to describe the crystal with a unit cell which is larger than the primitive unit cell. Although this makes the internal structure of the unit cell more complicated, it often makes the description of the whole crystal easier.

Most metallic crystals can best be described by a hexagonal or cubic unit cell (see figure 2). In the case of a cubic unit cell $\boldsymbol{a_1}$, $\boldsymbol{a_2}$ and $\boldsymbol{a_3}$ are orthogonal, and describe the three ridges of a cube with length a_0. All positions p within the cube can be described by a linear combination of these vectors:

$$p(a,b,c) = a \cdot \boldsymbol{a}_1 + b \cdot \boldsymbol{a}_2 + c \cdot \boldsymbol{a}_3 \qquad (9)$$

with a, b and c in the interval [0...1]. Positions within the unit cell are commonly described by only these parameters a, b and c, with the notation *(a,b,c)*.

Placing one single atom at the corner of the cube, i.e. at *(0,0,0)*, forms the so-called "Simple Cubic" structure (figure 2a). The unit cell contains exactly 1 atom, and has a volume of $(a_0)^3$. By adding one atom in the center of the cube,

at *(0.5,0.5,0.5)*, we form the so-called Body Centered Cubic (BCC) unit cell, which now contains 2 atoms (figure 2b). The crystal could be described by a smaller unit cell, containing only one atom, but the BCC unit cell is often preferred as it is more convenient description due to the orthogonallity of $\boldsymbol{a_1}$, $\boldsymbol{a_2}$ and $\boldsymbol{a_3}$. By placing one atom at the centre each face of the cube we get the Face Centered Cubic (FCC) unit cell (figure 2c). This unit cell contains 4 atoms (at *(0,0,0)*, *(0,0.5,0.5)*, *(0.5,0,0.5)* and *(0,0.5,0.5)*). Again, a smaller unit cell can describe FCC crystals, but for the same reasons as for the BCC unit cell the FCC description is often preferred.

These three types of crystals can be described as vertically stacked layers of atoms, each layer exhibiting a square pattern. Another type of crystals is made up of vertically stacked layers with a hexagonal pattern. If each subsequent layer is shifted with respect to the previous one, to ensure that the atoms of each layer fall exactly 'in between' the ones of the underlying layer, we call this a Hexagonally Closed Packed (HCP) structure (figure 2d). We call this an "abab" stacking to indicate that each layer is exactly equivalent to the one two layers

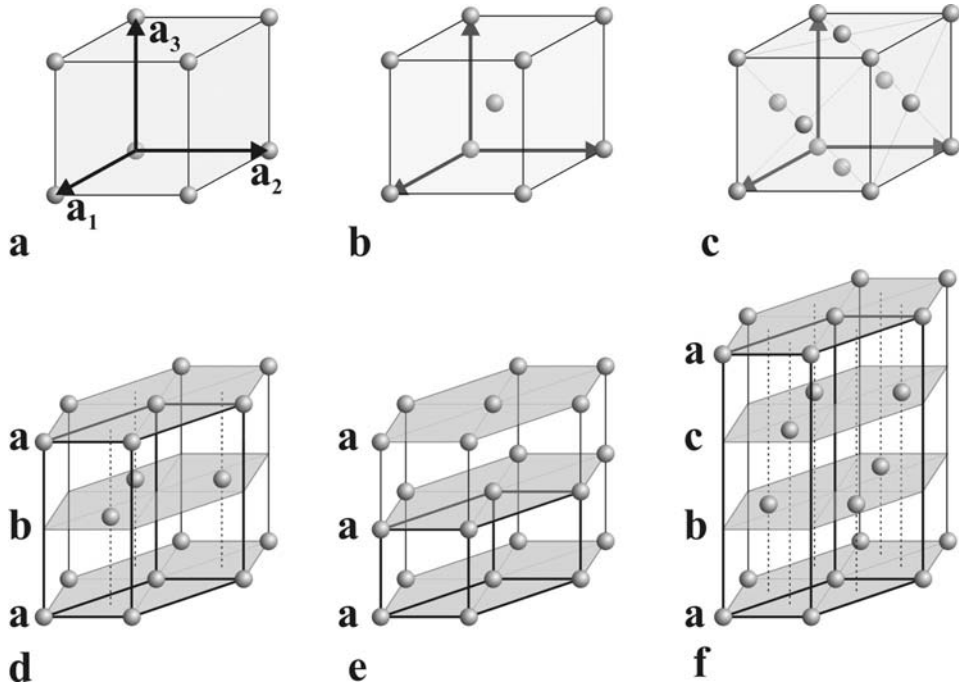

Figure 2: *3D crystal unit cells.* ***a)*** *Simple Cubic (SC),* ***b)*** *Body Centered Cubic (BCC),* ***c)*** *Face Centered Cubic (FCC),* ***d)*** *Hexagonal Closed Packed (HCP),* ***e)*** *'aaa' hexagonal stacking,* ***f)*** *abc stacking from a (111)-cut FCC crystal.*

below (or above). If all layers are exactly equivalent, i.e. all atoms are positioned exactly atop an atom from the layer below, we call this an "aaa" stacking (figure 2e). FCC crystals cut in a specific direction exhibit a hexagonal symmetry, and are characterized by an "abc" stacking, indicting that only one in three layers are really equivalent (figure 2f). A crystal of a certain volume inside which all unit cells are aligned with the same orientation is called a "single crystal". Crystals inside which one can find small volumes (crystallites) exhibiting different orientations are called "*polycrystalline*". If a crystal exhibits *all* unit cell orientations in equal amounts, it is referred to as a "*powder*". If a solid sample cannot be described by a unit cell, i.e. does not exhibit any periodicity in its structure, it is called "*amorphous*". In this thesis I will mainly concentrate on single crystals, and the surfaces of single crystals.

1.6.2: Cuts through crystal structures

Cutting an 'infinite' single crystal along a specific direction will create a "half infinite" crystal with a surface. We still consider the crystal to be infinite along the directions that are parallel to the surface, but half infinite in the direction perpendicular to the surface[v]. For this reason it is often convenient to describe the truncated crystal with a unit cell that has two out of the three vectors lying in the surface plane, and just one pointing out of the surface plane, i.e. perpendicular to the surface. This in contrary to the bulk unit cell, which, depending on the cut, might have more than one vector pointing out of the surface, would need a linear combination of all three vectors to define the surface plane. We hence define a unit cell with two vectors $\boldsymbol{a}$ and $\boldsymbol{b}$ to be the "in-plane" vectors, and **c** to be the "out-of-plane" vector. The area spanned by $\boldsymbol{a}$ and $\boldsymbol{b}$ is commonly called the "surface unit cell", and depends both on the specific cut of the crystal, and on the specific choice for $\boldsymbol{a}$ and $\boldsymbol{b}$. Even with this specific choice aimed at having a straightforward description of the crystallography of the surface, the bulk of the crystal is still correctly defined by the unit cell spanned by $\boldsymbol{a}$, $\boldsymbol{b}$ and $\boldsymbol{c}$; this newly chosen unit cell will commonly not coincide with e.g. the FCC or BCC bulk unit cell spanned by $\boldsymbol{a_1}$, $\boldsymbol{a_2}$ and $\boldsymbol{a_3}$.

[v] *Taking a simple cubic crystal and placing $\boldsymbol{a_1}$, $\boldsymbol{a_2}$ and $\boldsymbol{a_3}$ parallel to respectively $\boldsymbol{x}$, $\boldsymbol{y}$ and $\boldsymbol{z}$ in Cartesian coordinates, we cut the crystal along the (x,y)-plane. For simplicity we choose the surface to be at $\boldsymbol{z} = 0$. The truncated crystal has atoms occupying all available positions in $\boldsymbol{x}$ and $\boldsymbol{y}$ from $-\infty$ to ∞, but in $\boldsymbol{z}$ from $-\infty$ to 0 only. Hence the term 'half infinite'.*

All metal single crystal samples described later on in this thesis (Pt and Pd) have an FCC crystal structure. Because of this, I will limit the description of the surfaces and surface unit cells to the ones exhibited by truncated FCC crystals.

1.6.3: Low index planes

One way to describe the specific cut of a single crystal or equivalently its surface plane is by defining the surface normal vector ***c***. When this vector can be described by $a\cdot\boldsymbol{a_1}+b\cdot\boldsymbol{a_2}+c\cdot\boldsymbol{a_3}$ with *a*, *b* and *c* equal to 0 or 1 only, we call such a surface plane a "low index plane". For FCC crystals only three different low index planes exist. These three planes are usually denoted (001), (110) and (111). All other combinations of *a*, *b* and *c* equal to 0 or 1 give surfaces equivalent to these three. Figure 3 shows the cuts through the bulk unit cell which correspond to these three orientations. The (001), equivalent to (100) and (010), gives rise to a square surface unit cell with two perpendicular vectors ***a*** and ***b*** of length $1/\sqrt{2}\cdot a_0$ spanning its sides (figure 3a). The ***c*** vector points out of the surface plane and has a length of a_0. This bulk unit cell hence consists of two layers of atoms in this square configuration, shifted with respect to each other by (0.5 0.5 0.5)[vi].

The (110) surface (figure 3b) exhibits a rectangular surface unit cell with sides of respectively $1/\sqrt{2}\cdot a_0$ and a_0 . The **c** vector has a length of $1/\sqrt{2}\cdot a_0$, a_0 and again the bulk unit cell is composed of two atomic layers with this rectangular in-plane unit cell shifted with respect to each other by (0.5 0.5 0.5).

The (111) surface is the so called "closed packed" surface as it has the highest number of atoms per surface area (figure 3c). It has a diamond shaped surface unit cell, with an angle between ***a*** and ***b*** of 120 degrees, both vectors of length $1/\sqrt{2}\cdot a_0$. The **c** vector of length $\sqrt{3}\cdot a_0$ spans 3 layers of these hexagonal cells, shifted with respect to each other by respectively (2/3 1/3 1/3) and (1/3 2/3 2/3). Because of this 'tri-layered' structure this stacking of hexagonal layers is commonly called an "abc" stacking (see figure 3f). Of course, this specific choice of stacking order is slightly arbitrary, as a "bac" stack is not equal, but equivalent to an "abc" stack. If within one crystal these two types of stacking are mixed, we define the dominant type of stacking as

[vi] *These coordinates are with respect to the newly defined unit cell spanned by **a**, **b** and **c**, not the original bulk FCC unit cell.*

"abc", and the other one as the so-called "twin-stacking". One single transition from the normal stacking to the twin stacking is called a stacking fault.

1.6.4: Surface reconstructions

In some cases, the surface of truncated crystals is different from the cases stated here above. The surfaces discussed here above are all "bulk terminated", meaning that the surface atoms are all at the position one would expect them to be in an infinite crystal. Atoms in the bulk of a crystal are surrounded by a fixed number of neighboring atoms. Atoms in the surface plane of a crystal have less neighbors, as they miss all the atoms that would have been at z > 0 in an infinite crystal. Because of this, a surface can exhibit different properties than the bulk of a crystal. One of the effects that arise from the incomplete amount of bounds

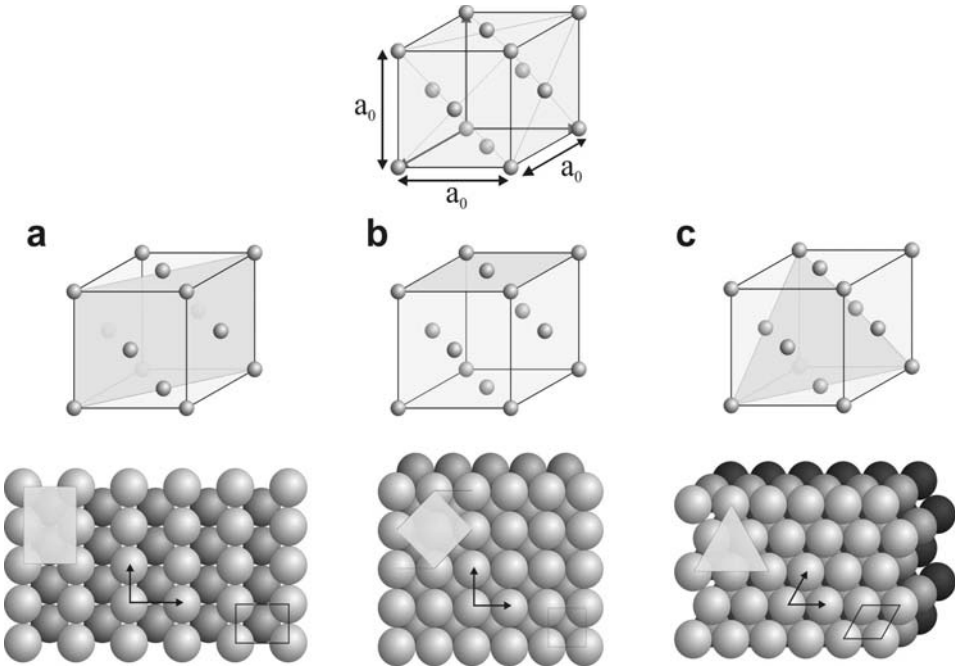

Figure 3: *Low index planes of an FCC crystal.* ***a)*** *the (110) surface exhibits a rectangular unit cell of a_0 by $a_0/\sqrt{2}$ (bottom right). This surface is equivalent to the $1\bar{1}0$. b) the (100) surface. This surface has a square symmetry, with a unit cell of $a_0/\sqrt{2}$ by $a_0/\sqrt{2}$ (bottom right). It is equivalent to the (001) and (010). c) The (111) surface exhibits a hexagonal symmetry. Taking deeper layers into account, this reduces to a 120-degree symmetry. The unit vectors can be chosen with an enclosed angle of 60 or 120 degree, but the resulting unit cell is always diamond shaped (bottom right) with sides of $a_0/\sqrt{2}$ by $a_0/\sqrt{2}$.*

with neighboring atoms is the build up of surface tension [31]. This surface tension is energetically (thermodynamically) unfavorable, and often surface atoms will change their configuration in order to try to minimize the surface tension. One way to achieve this is to shift the whole surface layer out- or inward with respect to the bulk atoms. Another way is to form a surface unit cell which is different from the one dictated by the bulk structure of the crystal, i.e. form a "reconstructed" unit cell. Several examples of this are the 7x7 reconstruction of the Si(111) surface [32], the hexagonal reconstruction of the Pt(001) surface, and the missing row reconstruction of e.g. the Pt(110) and Au(110) surfaces (see figure 4a) [33].

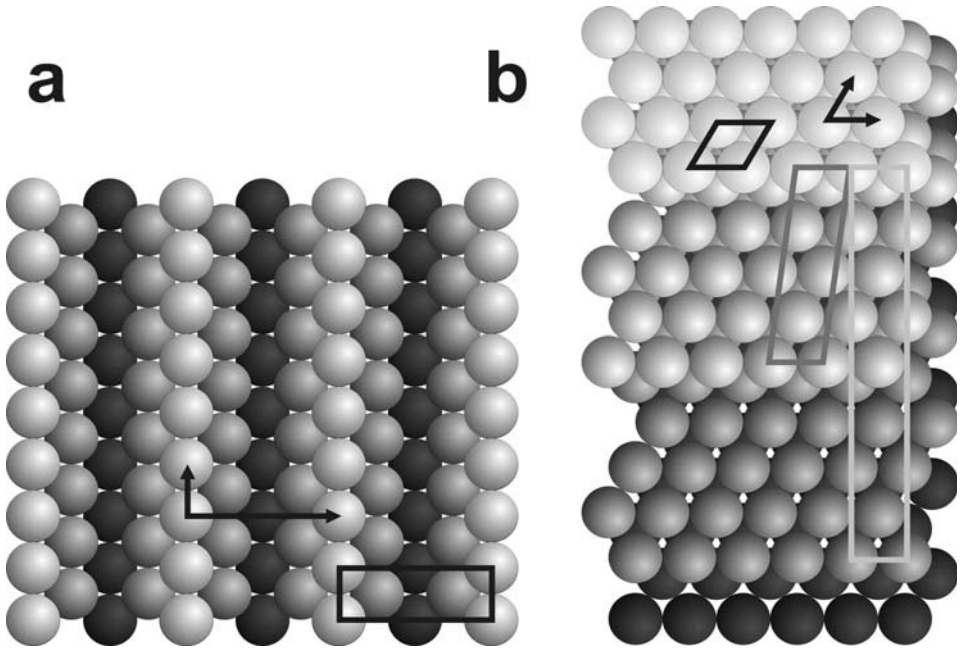

Figure 4: a) *A reconstructed (110) surface. The surface exhibits a 'Missing Row Reconstruction', which implies that every second row in the closed pack direction has been removed. With respect to the unreconstructed (110) surface, the unit cell (bottom right) is twice as long in the (001)-direction, and the surface layer contains only ½ of the bulk atomic density.* ***b)*** *The (553) surface. This is a high index surface, composed of 111 terraces and a regular array of* $11\bar{1}$ *steps. Different equivalent unit cells can be chosen to describe this surface. Two possible unit cells are drawn in (light gray, dark gray), next to the (111) unit cell and unit vectors (black).*

1.6.5: High index planes

Another type of more complicated surfaces are the so-called high index surfaces. By cutting a single crystal along a plane which is close, but not exactly equal to one of the low index planes presented here above we get a high index plane. These are surfaces of which the surface normal vector contains at least one values for *a*, *b* or *c* larger than 1, e.g. (553). A model of the (553) surface is shown in figure 4b. As we can see from the model, these surfaces are composed of terraces of the low index orientation closest to the normal vector of the surface, in this case (111). These terraces are separated by regularly spaced steps. One can choose different unit cells to describe this surface, of which two examples are shown in figure 4b in grey and light gray (in black the original (111) unit cell and vectors of the terraces). Both unit cells correctly describe the surface and bulk of the crystal. The choice for a certain unit cell is usually determined to facilitate either experiments or data analysis.

1.6.6: Altering surfaces: adsorption and growth

The description in 1.6.1 to 1.6.5 is a short introduction into the structure and surfaces of 'perfect' single crystals. In most experiments the surfaces of these crystals are prepared and cleaned under UHV to assure that they are as close to these theoretically perfect surfaces as possible. During the experiments though, these surfaces are exposed to a variety of circumstances, that will induce a change in the surface structure. In the experiments described in this thesis, we have exposed surfaces to elevated pressure and temperature conditions, and have investigated the change in structure, physical and chemical properties of the surfaces caused by these conditions.

When surfaces are exposed to gas molecules, the atoms and molecules from the gas phase will interact with the solid surface. As the surface atoms 'miss' their neighboring atoms at $\mathbf{z} > 0$, it is often energetically favorable to form a bond with an atom or molecule from the gas phase. The energy gain associated with the adsorption of a single molecule (or atom) to a surface is called the binding energy E_{ads}. Depending on the exact nature of the bonding between the surface and the molecule this process is called chemisorption (E_{ads} typically much larger than kT at room temperature) or physisorption (E_{ads} typically in the order of kT at room temperature) [31]. Looking back at the ball models of single

crystal surfaces presented in figures 3 and 4 we see that we can find several different 'high symmetry' sites within one unit cell, e.g. on top of a surface atom, or exactly in between two, three or four surface atoms. These high symmetry positions are often preferred sites for molecules to adsorb to. Different species of molecules have different preferred adsorption site within the unit cell. Figure 5 shows several of these preferred adsorption sites. Usually these specific adsorption sites can only accommodate one single molecule.

How often a molecule actually binds to the surface depends on the impingement rate (the number of molecules that collide with the surface per time unit) and the sticking coefficient. The sticking coefficient is a dimensionless number that gives the probability for a molecule colliding with a clean surface to actually adsorb instead of being scattered back into the gas phase. This number of course depends on many parameters: the specific molecule and surface that collide, the angle under which they collide, but also the temperature.

Ideal gas law dictates that at a pressure of 10^{-6} mbar and at room temperature the impingement rate for molecules with a mass around 30 atomic mass units (O_2, N_2, CO, NO etc) is equal to approximately 1 molecule per site per second. The "Langmuir" is the unit of exposure. Exposing a surface to this impingement rate for 1 second is equal to 1 Langmuir [3,4,31].

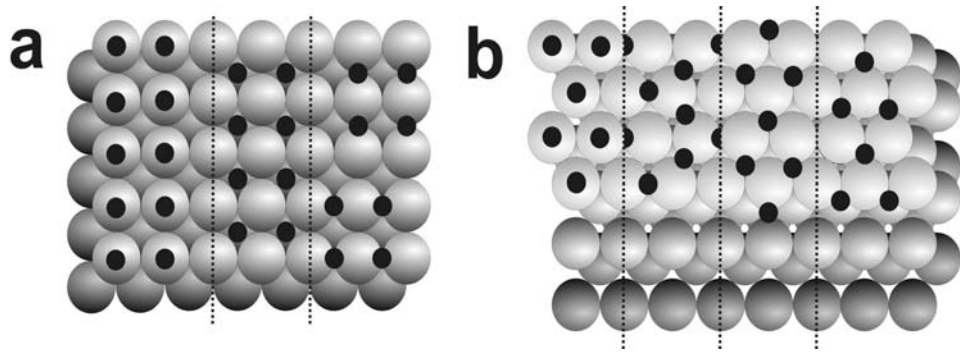

Figure 5: *High symmetry adsorption sites on a square and hexagonal surface.* ***a)*** *On a square lattice three possible adsorption sites would be the 'on top' positions (left), the '4-fold hollow' sites (middle) and 'bridge' positions.* ***b)*** *for a FCC (111) surface we again recognize 'on-top' positions (left), bridge sites (middle left), FCC threefold hollow sites (middle right) and HCP threefold hollow sites.*

The ratio between the adsorption energy of that specific molecule and the temperature of the surface (and hence of the adsorbed molecule) dictates how long a molecule will stay adsorbed on the surface before it spontaneously desorbs. The average time a molecule stays adsorbed on the surface is called the "mean stay time".

All these factors together determine how many molecules of a certain type are adsorbed on a certain surface at a given pressure and temperature. By dividing this by the total amount of available adsorption sites on that surface[vii] we get a number we call the "coverage" θ, which runs from 0 (a completely empty surface) to 1 (a fully occupied surface).

If the coverage gets significantly larger than 0, i.e. when many adsorbed molecules start having another adsorbed molecule as their neighbor, the molecules adsorbed on the surface will be influenced by each others presence. The combination of the specific adsorption energy at the different adsorption sites and this interaction will cause the adsorbed molecules to order themselves in a specific adsorption structure [34]. The unit cell of the adsorbed gas molecules often reflects the structure of the underlying metallic surface, and is usually denoted in units vectors of the (unreconstructed) metallic surface. Such a layer that forms on top of the single crystal surface and of which the unit cell can be described by a linear combination of the unit vectors of the substrate is called 'commensurate'. If the layer of adsorbed molecules can be described by unit vectors, but these vectors cannot be described by linear combinations of the substrate unit vectors, the layer of adsorbed molecules is called 'incommensurate'.

In the same manner as the adsorbed molecules feel the influence of the metal surface, the metal surface itself is influenced by the adsorption. The metallic surface atoms will rearrange in order to find the (energetically) most favorable position in presence of the adsorbed molecules. This might just imply that the surface atoms relax slightly outwards or inwards, depending on the potential of the bulk. But also more drastic rearrangements can take place, fully changing the surface unit cell [34]. The adsorption of molecules from the gas phase can make the surfaces form or loose a surface reconstruction.

[vii] *Often the total number of adsorption sites is set to 1 per atom of the bulk-terminated surface. This number is then calculated by dividing the total surface by the unit cell size, and multiplying by the number of atoms in the unit cell.*

If atoms from the gas phase are not only adsorbed on top of the surface, but diffuse into deeper layers of the crystal, forming a regular structure which contains both metallic and non-metallic atoms, we can no longer speak of adsorption. Depending on the particular species of atoms involved, these layers are referred to as ultra-thin oxides (metal-O), hydrides (metal-H), carbides (metal-C) or nitrides (metal-N). In many cases these “metal – non-metal” compounds have the structure and chemical composition one would expect from their bulk counterparts [5-7,9,10,13,23,35]. If they do not correspond to any known bulk structure or composition, they often get the preposition “surface-” to express that they only exist when formed at the metal-gas interface, i.e. the surface [36]. Again, these structures can form with a commensurate or incommensurate unit cell with respect to the substrate.

1.7: Surface X-Ray Diffraction

The main technique used in the experiments described in this thesis is Surface X-Ray Diffraction (*SXRD*). X-Ray Diffraction is a relatively old technique, pioneered by Von Laue and Bragg in the 1910's and 1920's [37,38]. It is one of the first applications of X-Rays for physicists. It is a structure sensitive technique: a crystal is illuminated by monochromatic X-Ray photons, which are then scattered (mainly) by the electrons in the crystal lattice. Because the photon are scattered by a regular array of electrons which reflects the crystal structure, the photons coming out of the crystal will create and interference pattern according to Bragg's law. From this pattern one can then try to calculate the position of the scattering centers, which corresponds to the crystallographic structure of the crystal.

With *Surface* X-Ray Diffraction the incoming photons have a glancing incidence angle α_i with respect to the crystal surface, typically smaller than 1°. Because of their limited penetration depth, the incoming beam of X-Rays will only illuminate a thin slice of typically 1 to 2 μm thick for a typical metal, measured in the direction perpendicular to the surface of the crystal[viii]. For low angles, the penetration depth scales approximately linearly with α_i.

Another advantage of illuminating a crystal at grazing incidence comes from the effect of total external reflection. This phenomenon occurs at the critical angle α_c, which is typically 0.2° for the combination of hard X-rays (in our case 17 keV) and metals. When α_i/α_c is near 1, the penetration depth drops rapidly to below 50 nm. This effect is strongly non-linear. [39,43].

1.7.1: SXRD from perfect crystal surfaces

If one illuminates a perfect, infinite single crystal with a monochromatic plane wave of X-Ray light, the light will be scattered by the electrons in the crystal. For *SXRD* we will only consider elastic scattering, implying that no energy is absorbed by the crystal due to the scattering process. Defining the incoming and

[viii] *The exact penetration depth depends strongly on the electronic density of the illuminated material, the wavelength of the incoming photons and the incidence angle. The value of 1 or 2 μm corresponds to the penetration depth in the lower en of the hard X-Ray regime (10 – 100 keV) at normal incidence for a typical metal like Fe or Ni multiplied by sin(α_i).*

outgoing X-Ray waves with wave vectors $\boldsymbol{k_{in}}$ and $\boldsymbol{k_{out}}$ respectively this mean that:

$$\left|\boldsymbol{k}_{in}\right| = \left|\boldsymbol{k}_{out}\right| \qquad (10)$$

Although the length of $\boldsymbol{k}$ is unchanged, the scattering process does change the orientation of $\boldsymbol{k}$. The difference between the incoming and outgoing vector is called the scattering vector (or momentum transfer) $\boldsymbol{q}$, and is defined as:

$$\boldsymbol{q} = \boldsymbol{k}_{out} - \boldsymbol{k}_{in} \qquad (11)$$

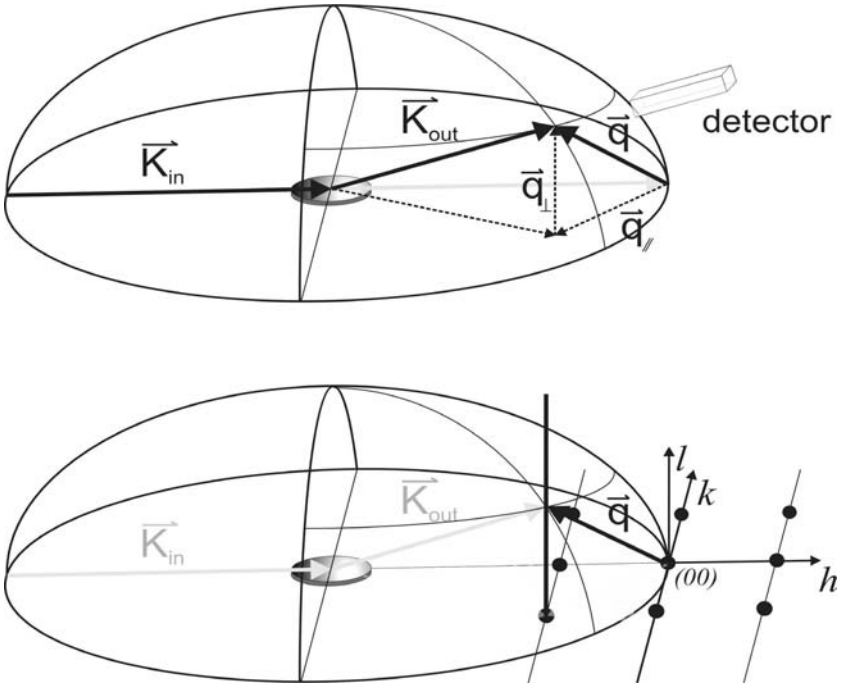

Figure 6: *Laue Diffraction geometry. Note that* $|\boldsymbol{K_{in}}| = |\boldsymbol{K_{out}}|$ *and* $\boldsymbol{q} = \boldsymbol{K_{out}} - \boldsymbol{K_{in}}$. $\boldsymbol{q}_{/\!/}$ *And* $\boldsymbol{q}_{\perp}$ *are respectively the in-plane an out-of-plane components of* $\boldsymbol{q}$. *The detector position determines the orientation of* $\boldsymbol{K_{out}}$. $\boldsymbol{q}$ *Determines if one will find diffracted intensity at that position according to equation 10.*

Figure 6 shows a graphical representation of equations (10) and (11). Not taking any crystal structure into account, we first define the electromagnetic (*EM*) field (the amplitude of the outgoing light) by the scattering of light from one single electron. This is described by the Thompson formula, i.e. the classical dipole radiation for an observer standing far from the source [17]. The amplitude of the scattered light E_s is given by:

$$E_s(\boldsymbol{r},\boldsymbol{q}) = -E_0 \frac{e^{-ikr}}{r} r_e \int \rho(\boldsymbol{r}) e^{i\boldsymbol{q}\cdot\boldsymbol{r}} d\boldsymbol{r} \qquad (12a)$$

In the case of e.g. a single electron $\rho(\boldsymbol{r})$ is a delta function at $r = 0$, and r_e is the classical electron radius. In the case of an atom, $\rho(\boldsymbol{r})$ is the electron density around the atom at position $\boldsymbol{r}$. As we are only interested in the dependence on $\boldsymbol{q}$ of the outgoing field, rather than its absolute amplitude, we will discard the factor outside the integral sign. This simplifies equation (12a) to:

$$E_q(\boldsymbol{r},\boldsymbol{q}) = \int \rho(\boldsymbol{r}) \cdot e^{i\boldsymbol{q}\cdot\boldsymbol{r}} d\boldsymbol{r} \qquad (12b)$$

In *SXRD* experiments the X-Ray beam does not interact with a single electron or atom, but with a periodic crystal composed of unit cells. In that case equations 4a and b describe the scattered electric field if $\rho(\boldsymbol{r})$ represents the local electron density of a single unit cell $\rho_{cell}(\boldsymbol{r})$. Equation (12b) now represents the Fourier transform of the local electron density of a unit cell and is commonly referred to as the structure factor F_q:

$$F_q = \int \rho_{cell}(\boldsymbol{r}) \cdot e^{i\boldsymbol{q}\cdot\boldsymbol{r}} d\boldsymbol{r} \qquad (12c)$$

If the scattering takes place in a regular periodic array of unit cells, such as the single crystal structures described previously, the scattered *EM* field can be calculated by the complex sum of the scattering amplitude F_q from the

individual unit cells. For an infinite single crystal with unit vectors $\boldsymbol{a_1}$, $\boldsymbol{a_2}$ and $\boldsymbol{a_3}$, and unit cells at ($n_1\boldsymbol{a_1}$, $n_2\boldsymbol{a_2}$, $n_3\boldsymbol{a_3}$), the scattered *EM* field is given by:

$$E_s(\boldsymbol{q}) = \sum_{n_1=-\infty}^{\infty} \sum_{n_2=-\infty}^{\infty} \sum_{n_3=-\infty}^{\infty} F_q e^{i\boldsymbol{q}\cdot(n_1\boldsymbol{a}_1+n_2\boldsymbol{a}_2+n_3\boldsymbol{a}_3)} \qquad (13a)$$

To calculate equation (13a) we can separate the scattering vector $\boldsymbol{q}$ into its three components $\boldsymbol{q_1}$, $\boldsymbol{q_2}$, and $\boldsymbol{q_3}$, lying along $\boldsymbol{a_1}$, $\boldsymbol{a_2}$ and $\boldsymbol{a_3}$. Equation (13a) then changes to:

$$E_s(\boldsymbol{q}) = \sum_{n_1=-\infty}^{\infty} \sum_{n_2=-\infty}^{\infty} \sum_{n_3=-\infty}^{\infty} F_q e^{i(n_1q_1a_1+n_2q_2a_2+n_3q_3a_3)} \qquad (13b)$$

The sum will be infinite for:

$$q_i \cdot a_i = n \cdot 2\pi \qquad \text{with } n = (0,1,2\ldots) \qquad (14a)$$

and *0* in all other cases. This non-zero condition is fulfilled for:

$$\boldsymbol{q} = 2\pi\boldsymbol{H} \qquad \text{with } \boldsymbol{H} = (h\boldsymbol{b_1} + k\boldsymbol{b_2} + l\boldsymbol{b_3}) \qquad (14b)$$

$$\text{and } h,k,l = 0,1,2,\ldots$$

with the vectors $\boldsymbol{b_i}$'s defined by:

$$\boldsymbol{a_i} \cdot \boldsymbol{b_j} = \delta_{ij} \qquad (14c)$$

The scattered intensity for an infinite perfect crystal will hence be infinite at $\boldsymbol{q} = 2\pi\,(h\boldsymbol{b_1} + k\boldsymbol{b_2} + l\boldsymbol{b_3})$[ix] and *0* elsewhere. These vectors $2\pi\boldsymbol{b_1}$, $2\pi\boldsymbol{b_2}$ and $2\pi\boldsymbol{b_3}$ are called the reciprocal lattice vectors and their linear combinations point out all the Bragg peaks, i.e. all positions in reciprocal space where one can find diffracted intensity. This shows that we detect $\boldsymbol{k_{out}}$ (see figure 6), but that the intensity of the outgoing X-Rays is determined by $\boldsymbol{q}$. It is common to define positions in reciprocal space by just the values of *h*, *k* and *l*, with the notation *(h k l)*. The axes that span reciprocal space are often referred to as the *h*-, *k*- and *l*-axis [30] (figure 7A). As mentioned earlier, it is often more convenient to define a truncated crystal with a different unit cell than the bulk unit cell used for infinite crystals, substituting $\boldsymbol{a_1}$, $\boldsymbol{a_2}$ and $\boldsymbol{a_3}$ for $\boldsymbol{a}$, $\boldsymbol{b}$ and $\boldsymbol{c}$. Normally $\boldsymbol{a}$ and $\boldsymbol{b}$ are chosen such that they lie in the surface plane of the crystal. Automatically $\boldsymbol{c}$ is then perpendicular to the surface plane. The corresponding reciprocal vectors will exhibit the same symmetry. The *l*-axis is perpendicular to both $\boldsymbol{a}$ and $\boldsymbol{b}$ and hence perpendicular to the surface. In turn, *h* and *k* span a plane which is parallel to the crystal surface (figure 7A). The diffracted intensity distributed in the *(hk)*-plane at $l = 0$ is called in-plane intensity and reflects the symmetry of the unit cell within the layers of the crystal. The diffracted intensity that is distributed along *l* at each integer *(hk)* point is called the out-of-plane intensity, or "crystal truncation rod" (CTR) (see figure 7A and C)

1.7.2: Non perfect crystals and surfaces: CTRs

Real life single crystals used in *SXRD* experiments are never truly perfect and infinite. Consequently, the sum of equation (13a) will in real experiments never result in perfect delta peaks, but always in peaks of non-zero width. The exact distribution of the diffracted intensity as a function of *h*, *k* and *l* reflects the deviations from the perfect infinite crystal.

In the case of a truncated crystal, the crystal is no longer infinite but 'half infinite' and exhibits a surface. With the crystal surface at $n = 0$, the sum in equation *(5)* in the direction perpendicular to the surface will hence not run

[ix] *Extinction effects due to unit cells with multiple atoms are omitted for this description.*

from $n = -\infty$ to $n = \infty$, but only from $n = -\infty$ to $n = 0$[x]. If we also include the finite penetration depth of X-Rays inside the crystal in the direction perpendicular to the surface due to the absorption μ, equation 5 can be rewritten as:

$$E_s(\boldsymbol{q}) = \sum_{n_1=-\infty}^{\infty} \sum_{n_2=-\infty}^{\infty} \sum_{n_3=-\infty}^{0} F_q e^{i(n_1 q_1 a_1 + n_2 q_2 a_2) + i n_3 q_3 a_3} \cdot e^{a_3 n_3 / \mu} \qquad (13c)$$

with $\boldsymbol{a_3}$ the vector pointing in the direction perpendicular to the surface. The terms containing $\boldsymbol{a_3}$ form the out-of-plane diffraction. Because the sum of n_3 only runs from $-\infty$ to 0, the intensity at non integer l-values will not be completely extinct. The smeared intensity distribution along l at integer *(hk)*-values due to the truncation of the crystal form a Crystal Truncation Rod (CTR). The intensity at the Bragg peaks is now no longer infinite. It depends on the exact energy of the X-Rays, the absorption of the crystal at that energy, the incident and outgoing angle of the X-Rays and the 'quality' of the crystal bulk. The lowest intensity point of a CTR, exactly in between two Bragg peaks is called the anti phase point, as this is the point at which the diffraction signal from two subsequent layers has a phase difference of exactly π, i.e. is out of phase. Due to the presence of the surface, and the non-zero absorption of the X-Rays, the intensity of the diffraction signal at that point is equivalent to that exactly 0.5 monolayer (ML) of the crystal for bulk terminated surfaces [39,43]. Due to its relatively low intensity, the diffraction signal at this point in reciprocal space is sensitive to small changes in the crystals (surface) structure.

All experiments presented in this thesis were performed at 17 keV photon energy and with late transition metal crystals. The ratio of the diffracted intensity between the Bragg peaks and the anti phase point was approximately 10^5. Depending on the incident flux of photons, this resulted typically in a signal of 10^{10} photons / sec at the detector for the Bragg peaks, and 10^5 at the anti phase. Due to the stochastic nature of the scattering of light, the error bar is in the order of the square root of the number of photon counts. A change in the

[x] *In a more general case, the surface need not be at n = 0, but will be at n = N, with N an arbitrary integer. It is however straightforward to change n to n' = (n-N), such that the surface is a n' = 0. The sum of equation (5) will hence run from n' = (-∞-N) to n' = 0 which is equal to the same sum running from -∞ to 0. This effectively means that we can always choose a value for n' such that the surface of the crystal is at $n_3 = 0$.*

crystal structure involving a fraction of a monolayer is hence invisible in a Bragg peak, but easily detectible at the anti phase point.

With the present intensities and photon flux available at modern X-Ray Synchrotron sources, changes in the crystals structure as a relaxation of the outermost atomic layer of only a fraction of a unit cell is easily detectible around the anti phase point of single crystals. Also the formation of roughness or deposition of material in the sub-monolayer regime can be very accurately

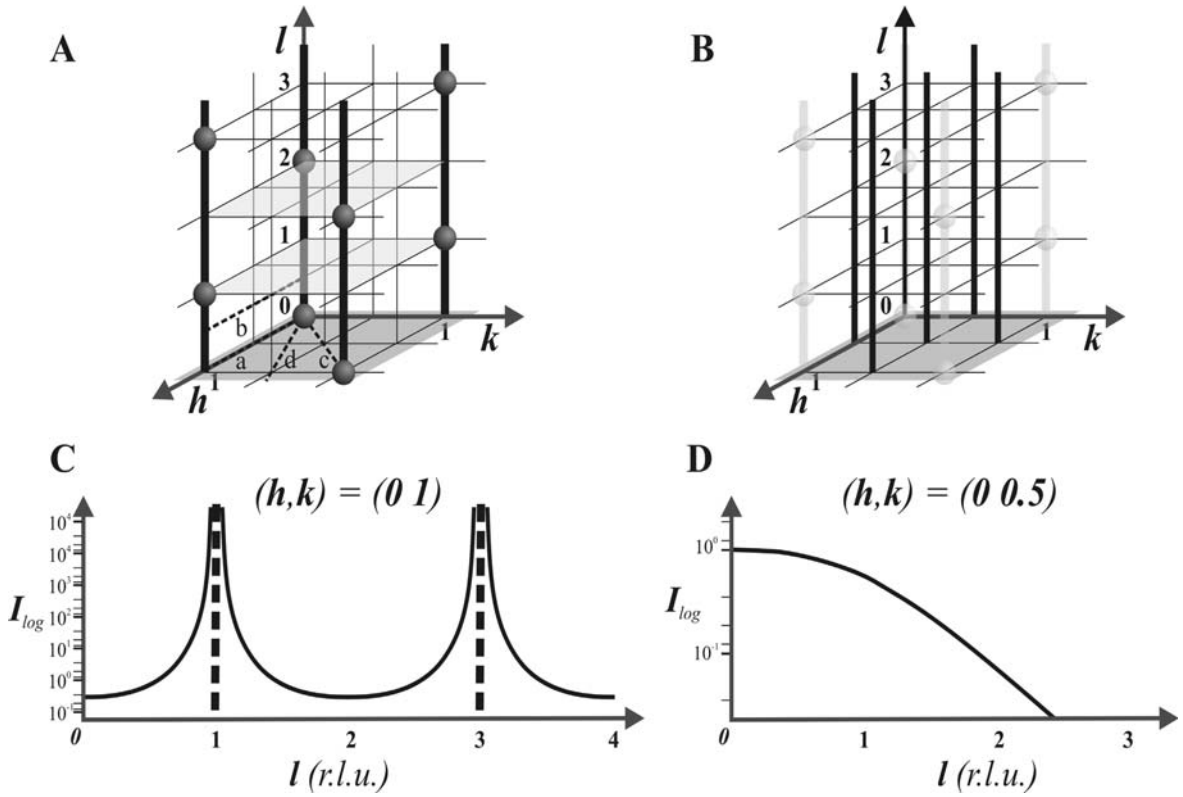

Figure 7: ***A)*** *Crystal Truncation Rods in reciprocal space. The Bragg peaks are marked as black dots along the rod. a, b, c and d represent different typical (hk) scans through reciprocal space. 'a' would be the perfect in-plane scan along h. Due to the finite incidence and exit angle necessary our diffraction geometry, a scan along l = 0 is not attainable. 'b' is the attainable version of an in-plane h-scan at l = 0.5. 'c' and 'd' are examples of in-plane 'radial' scans along respectively h = k and h = 2k.* ***B)*** *Half-order or reconstruction rods at non-integer values of h and k (black lines) (CTRs from (A) are shown in light grey for reference).* ***C)*** *The CTR at h = 0 and k = 1 for e.g. a BCC crystal. Bragg peaks showing at l = 1, 3… and anti-phase points at l = 0, 2, 4… .* ***D)*** *A typical diffraction signal for a single layer structure e.g. a surface reconstruction. As there is no interference with any other atomic layer in the out-of-plane direction, the diffraction signal shows no maxima or minima.*

measured with *SXRD*. Furthermore, the exact shape of the CTR scans is built up from the interference of many atomic layers of the crystal, and will therefore contain information about the content of these layers buried inside the crystal, e.g. stacking faults, impurities or alloying and in general the length of the ordered domains in the direction perpendicular to the crystal surface.

If a crystal surface exhibits a reconstruction or an adsorbed gas layer with a periodicity which is different than that of the original bulk or surface lattice, diffracted intensity will appear in reciprocal space at non-integer values of h and k. The intensity distribution along l arising from these structures will again form rods. These are called "reconstruction rods", or "non integer rods". These rods contain no Bragg peaks, as they have no contribution from a bulk crystal, but only from one single layer of atoms. The quality of *SXRD* data gathered at synchrotrons is nowadays such that even light molecules with low electron density adsorbed on the surface in an ordered lattice will form reconstruction rods of measurable intensity [17].

1.7.3: Calculating structures from SXRD

According to equations (12) and (13) it should be possible to calculate F_q from the scattered *EM* field $\boldsymbol{E(q)}$. It would then be possible to determine the electron density and thus the position of the atoms inside a crystal from a diffraction experiment. In order to do this it would be necessary to determine both the intensity as well as the phase factor of the scattered electric field, i.e. the factor $e^{(i\mathbf{qr})}$ from equations (12) and (13). Unfortunately it is in many cases not possible to determine the phase of the scattered *EM* field but only the scattered intensity $\boldsymbol{I(q)}$, which is equivalent to $|\boldsymbol{E(q)}|^2$ [17]. Consequently it is only possible to determine $|F_q|^2$. Because of this it is usually not possible to directly determine the crystal structure from the measured *SXRD* data. Structures are commonly solved by starting with an educated "guess structure", and simulating the diffracted intensity $\boldsymbol{I(q)}$ that would arise from that structure. The simulated data is then compared to the measured data, and the original input structure is adjusted to improve the fit between the measured data and simulated data. The structure that fits the original data best is then determined by iteration. It is possible to automate that process and let a fitting procedure minimize the (numerical) difference by e.g. a χ^2 minimalization. All structures presented in this thesis have been determined in this way and the fits have been performed

with the software package ANA / ROD [41]. In a more direct way, the size, orientation and enclosed angles of a unit cell is determined by the position of the diffraction maxima of that specific structure.

Whereas the position and intensity of the diffraction peaks measured in reciprocal space allow scientists to determine the crystal lattice and internal structure of the unit cell, other features of the diffracted peaks can be analyzed to give additional (morphological) information about the sample. The Full Width at Half Maximum (*FWHM*) of a diffraction peak will typically scale with the inverse of the length of the atomically ordered area from which the light is scattering. A simple formula gives a fairly good approximation [42]:

$$\Delta \boldsymbol{q}_{fwhm} = \frac{c}{L} \qquad (15)$$

where L is the average length of the ordered area, $\Delta \boldsymbol{q}$ is the *FWHM* of the diffraction peak in reciprocal length units and c is a constant that depends on the specific peak shape. This formula is not always valid. For example with very sharp peaks the instrumental resolution can strongly influence the

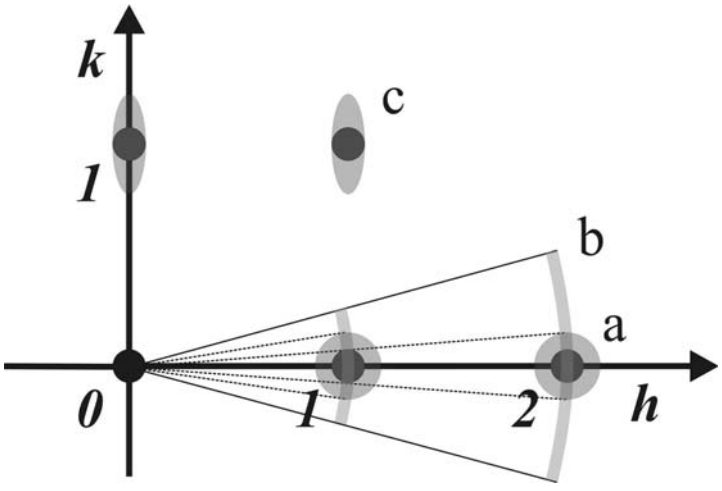

Figure 8: *In-plane diffraction map of a square lattice (black dots). The larger grey spots 'a' show the effect of diminishing domain size. 'b' shows the effect of mosaïcity. If the domain size is systematically different in different directions in real space, this will also be reflected in the spot size and shape, as shown at 'c'.*

measured full width of a peak. For volume Bragg peaks of high quality single crystals this formula also fails. There the *FWHM* will mainly be determined by the penetration depth of the X-Rays, and the diffraction will show more influence of multiple scattering. Not only the domain size will influence the *FWHM* of a diffraction peak, also the (mis-) orientation of different domains (mosaïcity) with respect to each other will change the measured *FWHM*. Figure 8 shows the effect of different types of disorder on the *FWHM* of a few in-plane diffraction peaks [43].

Scanning, or measuring the diffracted intensity, along different directions in reciprocal space will give different information about the structure of the sample (see figure 9). The most typical scans that are performed during an *SXRD* experiment are:

6) Scans along *l* at integer (CTR) or non-integer positions of the *(hk)* plane. These give information about the out-of-plane ordering of the sample (figure 9A and B).

7) Scans along *h*, *k* or a combination thereof. These give information on the in-plane structure of the sample (figure 9C).

8) Rocking scans around the surface normal: Depending on the *(hkl)* position these contain similar information as scans along *h* or *k*, but with the advantage that the sample moves instead of the detector. By scanning only the crystal lattice with respect to $\boldsymbol{q}$ instead of scanning both $\boldsymbol{q}$ and $\boldsymbol{k}_{out}$, this type of scans contains information about the crystal structure with a minimum of influence from the instrumental parameters (figure 9E).

9) Scans along *(00l)*. These are commonly called reflectivity scans. The CTR at *(hk) = (00)* can be considered as any normal CTR, with the exception that $\boldsymbol{q}_{in\text{-}plane} = 0$. This makes this scan completely insensitive for the in-plane (dis)ordering of a sample, yielding information about the out-of-plane electron density only (figure 9D).

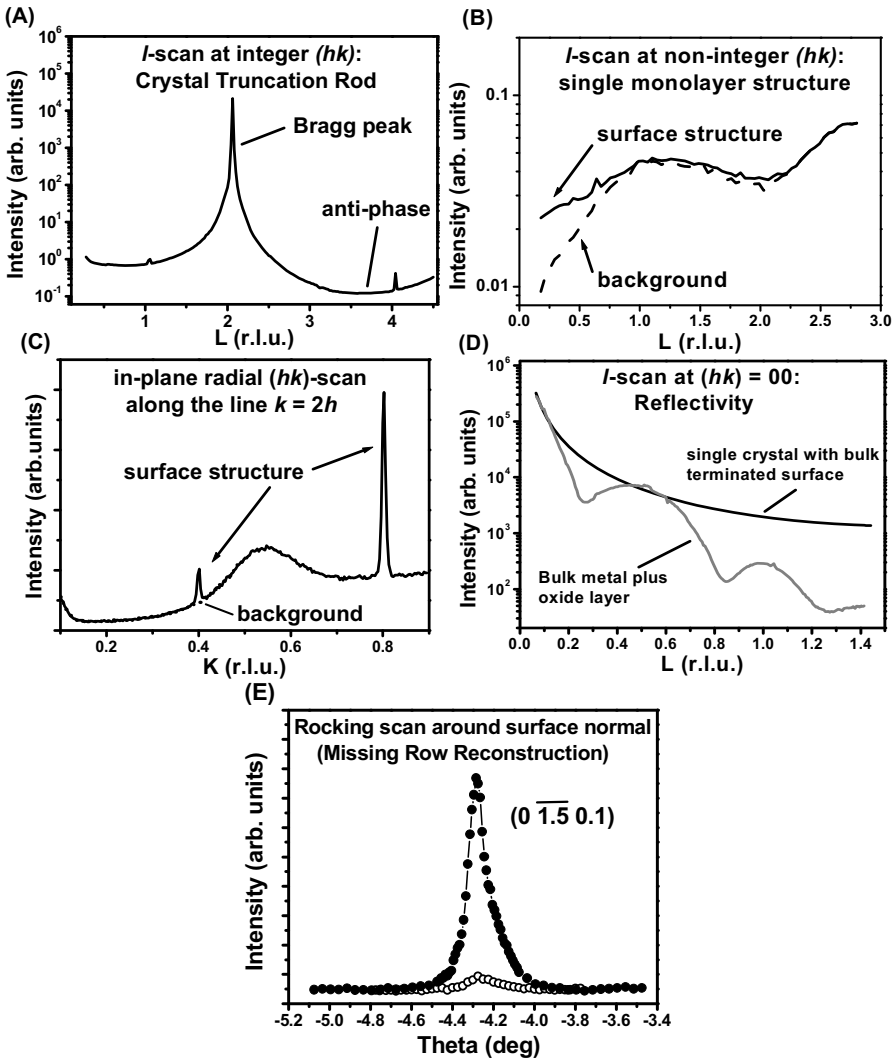

Figure 9: *Several examples of SXRD scans.* ***(A)****: A Crystal Truncation Rod of a clean, in-vacüo prepared Pt(111) single crystal, showing one Bragg peak (at l = 2) and two anti-phase positions (l = 0.5 and l = 3.5).* ***(B)****: A scan along l at a non-integer position, containing the diffracted intensity from only one single atomic layer. The diffraction signal (with respect to the background intensity) only shows intensity at low l values, and exhibits a smooth decrease as a function of l.* ***(C)****: An in-plane radial scan along the line k = 2h and low l . The scan shows peaks from a surface structure at non integer positions.* ***(D)*** *The reflectivity or l-scan at (hk) = (00). The reflectivity curve from a clean, bulk terminated crystal is shown (black line), and the reflectivity of that same crystal covered with only a few atomic layers of an oxide on top of the surface.* ***(E)*** *Rocking scan around the surface normal of the Missing Row Reconstruction on Pt(110) before and after exposure to CO. From the width of the peak a domain size and shape can be calculated. From the integrated intensity we calculate the fraction of the surface which is reconstructed.*